Heliyon

ELSEVIER

Received:
11 November 2018
Revised:
18 January 2019
Accepted:
21 January 2019

Cite as: Himanshu Joshi, D. P. Rai, Lalhriatpuia Hnamte, Amel Laref, R. K. Thapa. A theoretical analysis of elastic and optical properties of half Heusler MCoSb (M=Ti, Zr and Hf). Heliyon 5 (2019) e01155. doi: 10.1016/j.heliyon.2019.e01155

A theoretical analysis of elastic and optical properties of half Heusler MCoSb (M = Ti, Zr and Hf)

Himanshu Joshi [a], **D. P. Rai** [b,c,*], **Lalhriatpuia Hnamte** [a], **Amel Laref** [d], **R. K. Thapa** [a,e]

[a] *Condensed Matter Theory Research Group, Department of Physics, Mizoram University, Aizawl, Mizoram 796004, India*

[b] *Division of Computational Physics, Institute for Computational Science, Ton Duc Thang University, Ho Chi Minh City, Vietnam*

[c] *Faculty of Electrical and Electronics Engineering, Ton Duc Thang University, Ho Chi Minh City, Vietnam*

[d] *Department of Physics, College of Science, King Saud University, Riyadh, Saudi Arabia*

[e] *Condensed Matter Theory Research Centre, Butwal, Rupendehi, Nepal*

[*] Corresponding author.

E-mail address: dibya@tdt.edu.vn (D.P. Rai).

Abstract

Ab initio calculation of the Elastic and Optical properties of cubic half-Heusler compounds MCoSb (M = Ti, Zr and Hf) are reported using the FP-LAPW approach of the Density Functional Theory. Generalized Gradient Approximation was used as the exchange and correlation potential for investigating these properties. It was found that the Bulk modulus decreases with the increase in temperature and increases with the increase in pressure for all of the three Heusler compounds under study. The Debye's temperature along with compressional, Shear and average elastic wave velocities has also been calculated. The elastic results are compared with the available theoretical and experimental works. The optical investigation of the compounds shows high reflectivity at the infrared region of the photon energy. The imaginary part of the dielectric function reveled the optically non-metallic behavior of the MCoSb compounds, with optical band gap being around 1 eV.

https://doi.org/10.1016/j.heliyon.2019.e01155

Keywords: Materials science, Condensed matter physics

1. Introduction

Heusler compounds have made a tremendous contribution to the field of material science since its discovery in 1903. It is rather surprising that the number of potential applications Heusler compounds exhibit owing to their simple crystalline structure. They are one of the most studied compounds for half-metallicity, ferromagnetism, superconductivity, Hall effect and thermoelectricity [1]. These compounds also possess high Curie temperature along with high spin-polarization, which is of great importance in technological applications. The potentiality of a Heusler compound for a particular type of application can be easily determined by counting their valence electrons. Heusler compounds with a valence electron count (VEC) of 18 or 24 are narrow band semiconductors and are potential thermoelectric materials [2]. VEC other than 18 or 24 makes these compounds half-metallic in nature. Most Heusler compounds with VEC of 19 or 22 are half-metallic ferromagnets which is favorable for spintronic applications [3, 4, 5]. Heusler compounds which are non-magnetic and have a VEC of 27 or 18 are found to be superconductors [1, 6]. Therefore, due to their vast technological applications new Heusler compounds are in continuous demand. Some new Heusler compounds which were theoretically found to be stable violated the stability criterion when synthesized experimentally, thus arising a serious concern about stability from theoretical approach [7]. One of the method to ensure the stability of a structure through theoretical calculations is to check its mechanical stability which according to Born [8] is a necessary condition for thermodynamic and structural stability. Thus, the role of elastic constants is important to determine the mechanical stability in order to further verify the stability criterion and the order parameter of a structure [9]. Very few experimental and theoretical works are available on the investigation of elastic properties of these compounds. Sekimoto *et al.* (2005) [10] had experimentally investigated the sound velocities, Debye's temperature and the Young's modulus of the materials. Unfortunately, no other experimental works on the elastic properties of the compounds are reported on the available literature. Coban *et al.* (2016) [11] had theoretically investigated the elastic constants of HfCoSb within DFT formulation. The elastic constants of other two compounds are not known yet. Most of the works reported on these compounds are on their electronic and thermoelectric properties. However, elastic properties being one of the fundamental properties, its knowledge is essential as they provide information about the nature of bonding forces and the mechanical strength of the system which is of great importance for applications under different constraints. Therefore, we have made a detailed investigation on the elastic properties of half Heusler (HH) TiCoSb, ZrCoSb and HfCoSb from first principle method using the code ElaStic [12], based upon Density

https://doi.org/10.1016/j.heliyon.2019.e01155

Functional Theory (DFT) [13, 14]. Further, we have also calculated the Bulk modulus and Debye's temperature of the three HH compounds MCoSb employing Gibbs package [15, 16] based upon quasiharmonic Debye's approximation for better comparison purpose. All the three compounds were found to be mechanically stable as they satisfy the Born-Huang stability criteria [17] given by $C_{11} > 0$, $C_{44} > 0$, $C_{11} - C_{12} > 0$ and $C_{11} + 2C_{12} > 0$.

Optical properties of the compounds are also reported in addition to the elastic properties. These compounds still lack optical studies and experimental works are encouraged due to their non-availability. Optical parameters like the real and imaginary dielectric constant, refractive index, reflectivity, extension coefficient and the energy loss functional were investigated as a function of photon energy. It was found that the optical band gap in case of HfCoSb is higher than TiCoSb and ZrCoSb and varies as HfCoSb > ZrCoSb > TiCoSb. All other static optical parameters calculated varies in a reverse way with TiCoSb as highest and HfCoSb as lowest. HfCoSb has the highest energy band gap among MCoSb (M = Ti, Zr and Hf) and is the reason to also have highest optical gap. TiCoSb had the least band gap and also has the least optical gap. Our calculated energy band gap values were 1.04 eV, 1.073 eV and 1.137 eV respectively for TiCoSb, ZrCoSb and HfCoSb from Generalized Gradient Approximation (GGA) [18] energy exchange functional. The compounds under investigation being semiconductors, their intra-band transitions were neglected in the study of optical properties.

In this work, we have mainly focused on the theoretical investigation of elastic and optical properties of HH MCoSb. The investigated properties revel the fundamental nature of a material from which other characteristics can be extracted and is thus given importance in this paper. Elastic properties of Ti and Zr based MCoSb and the optical properties of ZrCoSb are being reported for the first time to the best of our knowledge.

2. Calculation

The lattice constants were calculated by a volume optimization method based upon Murnaghan's equation of state [19] and were performed using the WIEN2k code [20]. The code is based upon the Full Potential Linearized Augmented Plane Wave (FP-LAPW) approach of the Density Functional Theory. The lattice constants which were obtained and used in the calculation are respectively 5.8839 Å, 6.0912 Å and 6.0574 Å for TiCoSb, ZrCoSb and HfCoSb. They are found to be in close agreement with the experimental values [21, 22, 23, 24, 25]. Perdew–Burke–Ernzerhof Generalized Gradient Approximation (PBE-GGA) [17] was used to define the electron energy exchange and interactions. In order to fulfill a good convergence criterion, 10,000 optimized k-points were integrated in the first Brillouin zone to generate a $20 \times 20 \times 20$ Monkhorst-Pack mesh, with energy convergence set to 10^{-5} Ry and

https://doi.org/10.1016/j.heliyon.2019.e01155

charge to 10^{-3} e^{-}. The energy cut-off between the valence and the semi-core states was set to -8.0 Ry and were treated ignoring the spin-orbit coupling i.e. the semi-core states were treated semi-relativistically. The number of plane waves was set by limiting $R_{MT} \times K_{max} = 7$ in the interstitial region and the charge density expansion was set to $G_{max} = 12$. The muffin-tin radii (R_{MT}) of different atoms in the unit cell was calculated by optimization method and the optimized values are Ti = 1.81230; Co = 2.01608; Sb = 2.28841 for TiCoSb, Zr = 2.34603; Co = 2.07325; Sb = 2.57325 for ZrCoSb and Hf = 2.57664; Co = 2.03498; Sb = 2.31289 for HfCoSb. The R_{MT} optimization curve is shown in Fig. 1.

The elastic properties are calculated within the DFT framework using the Lagrangian theory of elasticity, in which a solid is assumed to be an anisotropic and homogeneous elastic medium. The second order elastic constants are calculated using the energy-strain method, as implemented in the code ElaStic [12]. The structure under investigation has cubic symmetry, so there are three independent elastic constants: C_{11}, C_{12} and C_{44}. From the elastic constants, different elastic properties were calculated using the Voigt, Reuss and Hill averaging scheme [26, 27, 28]. Voigt's approximation assumes uniform strain in the structure whereas Reuss approximation assumes uniform stress. Elastic moduli under different averaging scheme are described here under as follows-

Bulk modulus, which is the measure of resistance to compressibility was calculated using the expression in Eq. (1)

$$B = \frac{1}{3}(C_{11} + 2C_{12}), \tag{1}$$

The bulk modulus for a cubic structure is same for Voigt, Reuss and Hill averages. Shear modulus is generally defined as the deformation that occurs in a solid when a force is applied to any of the parallel face while the other face opposite to the parallel face is kept fixed by other opposite forces. In Voigt average, the shear modulus for a cubical symmetry is given by Eq. (2)

$$G_V = \frac{C_{11} - C_{12} + 3C_{44}}{5}, \tag{2}$$

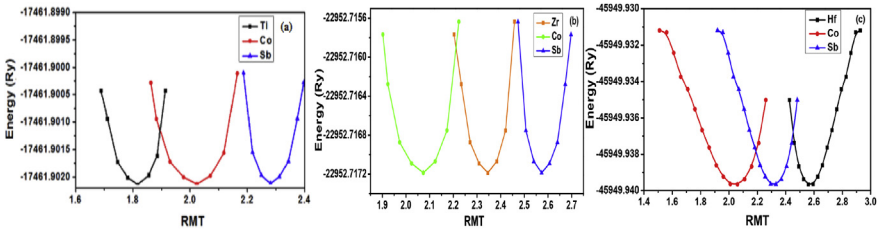

Fig. 1. R_{MT} optimization of (a) TiCoSb, (b) ZrCoSb and (c) HfCoSb.

https://doi.org/10.1016/j.heliyon.2019.e01155

The following expression shown in Eq. (3) gives the Reuss average

$$G_R = \frac{5(C_{11} - C_{12})C_{44}}{4C_{44} + 3(C_{11} - C_{12})}, \tag{3}$$

The arithmetic mean of the Voigt and the Reuss average in Eq. (4) gives the Hill shear modulus-

$$G_H = \frac{G_V + G_R}{2}, \tag{4}$$

The Young's modulus and the Poisson's ratio are calculated using Eqs. (5) and (6)

$$Y = \frac{9BG}{3B + G}, \tag{5}$$

$$\eta = \frac{3B - 2G}{2(3B + G)}, \tag{6}$$

Replacing G by G_V and G_R in Eqs. (5) and (6), one can calculate the Voigt and the Reuss average of Young's modulus and Poisson's ratio.

Debye's temperatures is calculated using Eq. (7), which is based upon Debye's assumption that the temperature of highest normal mode of vibration can be estimated from the average sound velocity [29].

$$\Theta_D = \frac{h}{k}\left[\frac{3n}{4\pi}\left(\frac{\rho N_A}{M}\right)\right]^{1/3} \upsilon_m, \tag{7}$$

here, h is the Plank's constant, k is the Boltzmann's constant, N_A is the Avogadro's number, n is the number of atoms per molecule or number of atoms per formula unit, M is the molar mass, ρ is the density of the unit cell and ν_m is the average sound velocity. The average sound velocity is further expressed in terms of compressional (ν_l) and shear (ν_s) sound velocities as given by Eq. (8) [30]

$$\upsilon_m = \left(\frac{1}{3}\right)\left[\frac{2}{\upsilon_s^3} + \frac{1}{\upsilon_l^3}\right]^{-1/3}, \tag{8}$$

The expressions for ν_s and ν_l is given by Eqs. (9) and (10) respectively

$$\upsilon_s = \sqrt{\frac{G}{\rho}}, \tag{9}$$

$$\nu_l = \sqrt{\frac{3B + 4G}{3\rho}}, \tag{10}$$

https://doi.org/10.1016/j.heliyon.2019.e01155

Elastic properties also relate to another physical parameter known as the shear anisotropy (A). It gives the nature of bonding in different crystallographic directions and is calculated using Eq. (11)

$$A = \frac{2C_{44}}{C_{11} - C_{12}}, \tag{11}$$

The elastic results are presented under "Results and Discussion" section that follows later in the paper and are compared with the results obtained using Debye's quasi-harmonic approximation employing Gibbs package.

The optical parameters calculated are the response of the compound MCoSb when electromagnetic radiation is introduced to them. The optical response of a material to an external electric field is given by its complex dielectric function$\varepsilon(\omega)$, which is defined by Eq. (12) as

$$\varepsilon(\omega) = \varepsilon_1(\omega) + \varepsilon_2(\omega), \tag{12}$$

where, $\varepsilon_1(\omega)$ is real and $\varepsilon_2(\omega)$ the imaginary part of the dielectric function $\varepsilon(\omega)$. The real and imaginary part of the dielectric function is calculated using the Kramers−Kronig relation [31] given by Eq. (13)

$$\varepsilon_1(\omega) = 1 + \frac{2}{\pi}\int_0^{\infty} \frac{\varepsilon_2(\omega)\omega^* d\omega^*}{\omega^{*2} - \omega^2}, \tag{13}$$

the momentum matrix elements between the occupied and unoccupied states gives the imaginary part of complex dielectric function

$$\varepsilon_2(\omega) = \frac{Ve^2}{2\pi m^2\omega^2} x \int d^3k \sum_{nn^*} \left|kn\middle|p\middle|kn^*\right|^2 f(kn) x\left[1 - f\left(kn^*\right)\right] \partial(E_{kn} - E_{kn^*} - \omega), \tag{14}$$

In Eq. (14), p is the momentum matrix element between n and n^* states, $|kn|$ is the crystal wave function while $f(kn)$ is the Fermi distribution function, E_{kn} is the eigen value corresponding to the crystal wave function $|kn|$. The refractive index $n(\omega)$and the extinction coefficient $k(\omega)$is calculated corresponding to Eqs. (13) and (14) using Eqs. (15) and (16) [32].

$$n(\omega) = \left(\frac{\sqrt{\varepsilon_1^2(\omega) + \varepsilon_2^2(\omega)} + \varepsilon_1(\omega)}{2}\right)^{1/2}, \tag{15}$$

$$k(\omega) = \left(\frac{\sqrt{\varepsilon_1^2(\omega) + \varepsilon_2^2(\omega)} - \varepsilon_1(\omega)}{2}\right)^{1/2}, \tag{16}$$

https://doi.org/10.1016/j.heliyon.2019.e01155

The optical properties are studied using the GGA energy exchange correlation functional.

3. Results and discussion

3.1. Elastic properties

The calculated elastic parameters are tabulated in Table 1. From the calculated elastic constant values, one can see that all the three compounds under investigation satisfies the stability criteria of Born-Huang as discussed earlier. Therefore, it is envisaged that the HH compounds MCoSb (M = Ti, Zr and Hf) are mechanically stable. For all of MCoSb, the C_{11} value is higher than C_{12} and C_{44}, which indicates that these compounds are hard to compress along the X-axes. The Bulk modulus values calculated from ElaStic code using Eq. (1) are respectively 147.59 GPa, 139.78 GPa and 144.68 GPa for TiCoSb, ZrCoSb and HfCoSb, which are very close to the values calculated from Murnaghan's equation of state (146.914 GPa, 139.865 GPa and 145.117 GPa). The similarity between the two results estimates the accuracy of elastic calculations. Our calculated Bulk modulus value of HfCoSb is higher than the theoretical report of Coban *et al.* (2016) [11] obtained from equation of state, which is 137.712 GPa. However, their Bulk modulus value obtained after elastic investigation is close to the one that we have calculated. Unfortunately for TiCoSb and ZrCoSb, no Bulk modulus results are available for comparison. Our calculated value of Young's modulus is 4.7% and 6.4% higher than the available experimental data for TiCoSb and HfCoSb, whereas for ZrCoSb, it is 2.4% lower. High value of Y in MCoSb shows that the covalent bonding component dominates these compounds. Strong covalent bond indicates that the material is stiff.

The fundamental parameter closely related to the melting point and specific heats in solid is the Debye's temperature. High Debye temperature indicates stiffer crystal orientation and such crystals are found to have high melting points. Debye temperature (Θ_D) being the temperature required to activate all the phonon mode of a

Table 1. Calculated elastic constants, Bulk modulus (B), Shear modulus (G), Young's modulus (Y) and Poisson's ratio (η)

Comp.	C_{11} *(GPa)*	C_{12} *(GPa)*	C_{44} *(GPa)*	G_V *(GPa)*	G_R *(GPa)*	G_H *(GPa)*	*B (GPa)*	*Y (GPa)*	*η*	*Ref.*
TiCoSb	254.8	94.0	88.4	85.20	85.02	85.11	147.59	205.36 196	0.26	This work [10], expt.
ZrCoSb	263.0	78.1	71.7	80.0	78.77	79.39	139.78	202.03 207	0.25	This work [10], expt.
HfCoSb	257.2	88.4	78.6	80.87	80.78	80.83	144.68	204.3 192	0.26	This work [10], expt.
	274.57	77.6	75.5			84.41	143.31	210.2	0.25	[11], theo.

https://doi.org/10.1016/j.heliyon.2019.e01155

crystal, large Θ_D values indicate high energy is required to excite the phonons in a crystal and such materials are highly favorable in thermoelectric power generation. In the compound MCoSb, the Debye's temperature varies as TiCoSb > ZrCoSb > HfCoSb and is found to agree with the experimental results of Li *et. al.* [33] and Sekimoto *et. al.* [10]. The Debye's temperature of ZrCoSb is in excellent agreement with the experimental values in reference 36, while TiCoSb and HfCoSb differs by 4.34% and 1.51% respectively. It is listed in Table 2. The calculated elastic wave velocities are higher than the available experimental results. The difference can be attributed to the temperature influence. The values that we report are observed at 0 K, whereas the values reported in experiments are observed in the temperature range of 300 K−900 K. Further, in theoretical calculations we consider perfect single crystals where as in experiments, crystal imperfection is taken into consideration which varies the two results. Our calculated values of A are 1.09, 0.76 and 0.93 for MCoSb (M = Ti, Zr and Hf) respectively. The calculated A values are either greater or less than 1 but not equal to. For any isotropic crystal, the value of A equals to 1. Values less than or greater than 1 is a measure of shear anisotropy possessed by the crystal. Thus HH MCoSb is purely anisotropic.

We have also calculated the unit cell density of MCoSb compounds and it was found that HfCoSb has the highest density among the three compounds investigated. The density is found to vary as HfCoSb > ZrCoSb > TiCoSb and the values are 10.7 g/cc, 7.9 g/cc and 7.4 g/cc respectively.

The plot of Bulk modulus is important as it alone can reveal the temperature and pressure characteristics of other moduli of elasticity and also that of elastic constants. We have used the quasiharmonic Debye's approximation to plot the variation of bulk modulus with respect to temperature at constant pressure, see Fig. 2 (a) and that with

Table 2. The compressional (ν_l), Shear (ν_s) and average (ν_m) elastic wave velocity in m/s, density (ρ) in g/cc, Debye's temperature (Θ_D) in K and the shear anisotropy (A) for MCoSb.

Comp.	ν_l *(m/s)*	ν_s *(m/s)*	ν_m *(m/s)*	ρ *(g/cc)*	Θ_D *(K)*	*A*	*Ref.*
TiCoSb	5918.413	3379.224	3755.187	7.453	435.08	1.09	This work
	5699	3237	–	–	417	–	[10], expt.
	5691	3230	–	–	416	–	[33], expt.
ZrCoSb	5544.085	3379.224	3503.823	7.991	392.073	0.76	This work
	5623	3192	–	–	399	–	[10], expt.
	5488	3134	–	–	392	–	[33], expt.
HfCoSb	4866.790	2766.790	3075.741	10.734	346.152	0.93	This work
	4743	2721	–	–	341	–	[10], expt.
	4703	2709	–	–	340	–	[33], expt.
	4841.62	2811.77	3119.98	–	220.77	0.77	[11], theo.

https://doi.org/10.1016/j.heliyon.2019.e01155

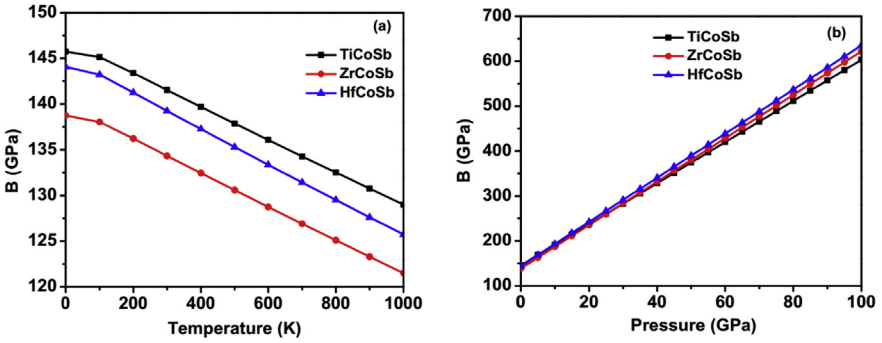

Fig. 2. Plot of bulk modulus with respect to (a) Temperature and (b) Pressure for MCoSb (M = Ti, Zr and Hf).

respect to pressure at constant temperature, see Fig. 2 (b). It is seen that the bulk modulus decreases abruptly with the increase of temperature. This indicates that the elastic constants C_{ij} will also decrease with the application of temperature. Thus, it can be predicted that all of the moduli of elasticity decreases with the increase of temperature at constant pressure. This abrupt decrease of *B* leads to an important property of HH compound MCoSb. That is, it shows the high temperature working range of these compounds because at high temperatures, due to the decrease of *B* and *G*, the *G/B* ratio will also decrease, making these compounds non-fragile at higher temperature ranges, which is a prime condition for number of applications like thermoelectricity, superconductivity etc. On the other hand, the pressure characteristics of Bulk modulus shows the disadvantages of the HH compound MCoSb at high pressure ranges. At constant temperature (0 K), *B* increases linearly with increase of pressure, thereby indicating the abrupt increase of elastic constants and thus the other moduli of elasticity. The boiling point and the melting point of the material also increases and thus gets cut out from number of applications like optical applications, solder applications etc. Further the *G/B* ratio also increases and thus the HH compound MCoSb becomes unfavorable for thermoelectric, superconductivity and other energy applications.

The value of B at 0 K, pressure remaining constant and that at 0 BPa, temperature remaining constant is very close to the B values listed in Table 1. Thus, it acts as an estimation of accuracy for results calculated from quasiharmonic Debye's approximation.

Similarly, using the same approximation, we have also calculated the Debye's temperature as a function of pressure and temperature using Eq. (17) [34].

$$\theta_D = \frac{\hbar}{k_B}\left(6\pi V^{1/2} n\right)^{1/3} f(\sigma)\sqrt{\frac{B}{M}}, \tag{17}$$

M is the molecular weight per formula unit and B is the bulk modulus which is assumed to be equal to the static bulk modulus as expressed by Eq. (18)

https://doi.org/10.1016/j.heliyon.2019.e01155

$$B = B_{static} = V\frac{d^2E(V)}{dV^2}, \tag{18}$$

The plot of $\theta_D$is shown in Fig. 3. From the figure it is seen that the $\theta_D$value decreases with the increase in temperature and increases with the increase in pressure. For TiCoSb and HfCoSb, where $\theta_D$was found to be higher than the experimental results from elastic calculation, whereas quasiharmonic calculations shows excellent agreement with the experimental results at 700 K and 500 K. The values obtained at different temperatures are listed in Table 3.

3.2. Optical properties

The investigation of optical properties is important in order to find the optoelectronic application of HH MCoSb. The optical properties are studied using the GGA energy

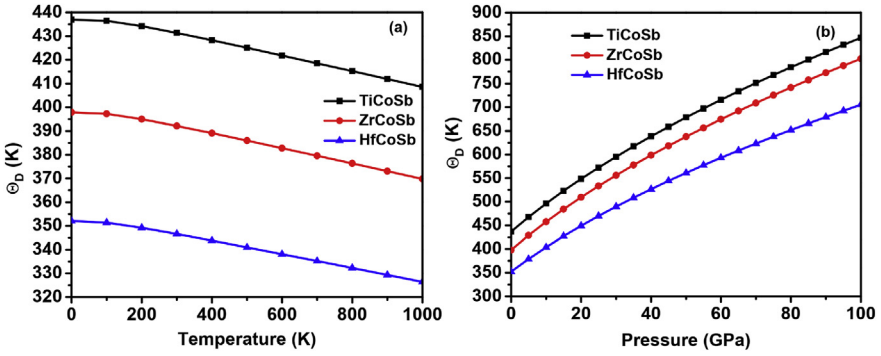

Fig. 3. Plot of Debye's temperature with respect to (a) Temperature and (b) Pressure for MCoSb (M = Ti, Zr and Hf).

Table 3. Debye's temperature calculated at different temperatures from quasiharmonic approximation.

Temperature (K)	*TiCoSb*	*ZrCoSb*	*HfCoSb*
0	436.94	397.84	352.05
100	436.43	397.25	351.4
200	434.23	394.98	349.21
300	431.37	392.13	346.58
400	428.27	389.08	343.81
500	425.07	385.95	340.97
600	421.81	382.77	338.1
700	418.52	379.56	335.21
800	415.21	376.33	332.3
900	411.88	373.08	329.37
1000	408.53	369.82	326.44

https://doi.org/10.1016/j.heliyon.2019.e01155

exchange correlation functional and the optical parameters are plotted in the energy range of 0−60 eV. Fig. 4(a) gives the plot of dielectric function $\varepsilon(\omega)$with respect to photon energy. Generally, there are two types of contribution to the dielectric function, inter-band transition and intra-band transition. The inter-band transition is further classified into direct inter-band transition and indirect inter-band transition. Usually, intra-band transition is prominent only in metals and our compound of investigation being a semiconductor, shows no intra-band transition. The indirect inter-band transition is negligibly small because electron excitation by photon across an indirect band gap is extremely rare due to low momentum of photons, when compared to the direct inter-band transition, thus we have neglected it in our calculation. The real part of the dielectric function shows sharp peaks at 1.78 eV, 1.92 eV and 1.91 eV respectively for TiCoSb, ZrCoSb and HfCoSb in the visible region of the spectrum. The obtained peaks are related with the nature of the functionals and can change with different functionals. After a peak value is obtained, the peaks reduces gradually and tends towards minimum value which is obtained at 8.61 eV, 6.35 eV, 6.08 eV respectively for TiCoSb, ZrCoSb and HfCoSb. This is due to the inter-band transition between the VCM and the CBM.

$\varepsilon_1(\omega)$increases from HfCoSb < ZrCoSb < TiCoSb, this is expected as the atomic radius increases from Ti < Zr < Hf. The static dielectric function $\varepsilon_1(0)$increases and attains the maximum value and then it declines until it attains a negative value for specific energy regions (3.578 eV-20.45 eV for TiCoSb; 3.932 eV−18.027 eV for ZrCoSb; 5.156 eV−18.925 eV for HfCoSb). There after $\varepsilon_1(0)$tends towards a constant value. The negative values indicates the reflection of incident radiation from the surface. Our calculated values of real part of static dielectric constants are respectively 21.505, 18.987 and 18.403 for TiCoSb, ZrCoSb and HfCoSb.

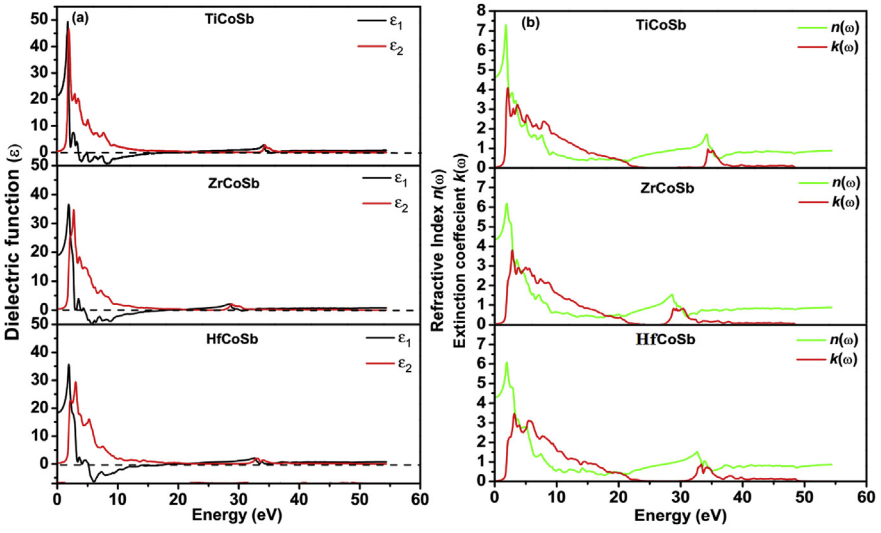

Fig. 4. (a) Real and imaginary parts (ε_1 and ε_2) of dielectric function (b) Dispersion curves of refractive index n (ω) and extinction coefficient k (ω).

https://doi.org/10.1016/j.heliyon.2019.e01155

Energy shift for the location of the peaks is observed in different MCoSb HH compounds but the general pattern of the $\varepsilon_1(\omega)$curves are similar to each other. The optical band gap of a compound is given by the zero frequency value of the imaginary part of the dielectric function, $\varepsilon_2(\omega)$. The calculated optical band gaps are 0.775 eV, 1.102 eV and 1.156 eV respectively for TiCoSb, ZrCoSb and HfCoSb. The value of this gap and the one calculated from band structure plots (Table 4) are close to each other, which verifies the reliability of the optical calculations. The peak values are obtained at 2.95 eV, 2.734 eV and 3.06 eV respectively for different components of MCoSb. This peaks originates due to the transition from 3*d*, 4*d* and 5*d* states of M and Co atom to the 5*p* states of Sb atom. A red shift is observed between TiCoSb − HfCoSb and HfCoSb − ZrCoSb as the peak values of $\varepsilon_2(\omega)$has shifted to lower energy range between these compounds.

The refractive index $n(\omega)$and the extinction coefficient $k(\omega)$is calculated using Eqs. (15) and (16), it is shown in Fig. 4 (b). The high peaks of the refractive index is observed in the visible region of the spectrum. The static refractive index obtained is 4.64, 4.36 and 4.29 for Ti, Zr and Hf components of MCoSb respectively and it increases from Hf to Ti. The static refractive index $n(0)$satisfies the relation$n\ (0)^2 \approx \varepsilon_1(0)$, which further verifies the accuracy of the calculation. It can be seen that the trends of $k(\omega)$is similar to that of $\varepsilon_2(\omega)$, it is because $k(\omega)$also provides a measure of absorption of incident radiation. The extinction coefficient $k(\omega)$becomes very low in the energy range between 0.0136 eV−1.7007 eV and between 23.088 eV−27.875 eV (the energy region being much wider for TiCoSb and HfCoSb). It indicates very low absorption of light which is favorable for transparent properties of the material in this range of the photon energy.

Reflectivity or reflection coefficient R(ω) is a measure of the amount of electromagnetic radiation reflected from the incident medium (Fig. 5a) and is calculated using Eq. (19) [32]

$$R(\omega) = \left| \frac{\sqrt{\varepsilon(\omega)} - 1}{\sqrt{\varepsilon(\omega)} + 1} \right|^2, \tag{19}$$

As an application of the external radiation incident on the material, some of the valence electrons may undergo inelastic scattering, leading to loss of energy. The energy lost by the electron can be calculated using Eq. (20)

Table 4. Calculated band gap (ΔE_G) for TiCoSb, ZrCoSb and HfCoSb.

Compound	TiCoSb	ZrCoSb	HfCoSb
ΔE_G *(eV)*	1.040	1.073	1.137

https://doi.org/10.1016/j.heliyon.2019.e01155

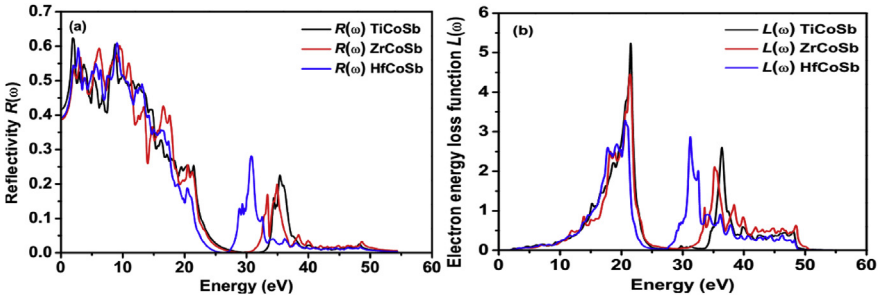

Fig. 5. Plot of (a) Reflectivity R (ω) and (b) Electron energy loss functional L (ω) vs Photon energy.

$$L(\omega) = -\mathrm{Im}\left\{\frac{1}{\varepsilon(\omega)}\right\} = \left(\frac{\varepsilon_2(\omega)}{\varepsilon_1^2(\omega) + \varepsilon_2^2(\omega)}\right), \tag{20}$$

The high peaks in the L(ω) vs energy plots represents the plasma resonance behavior (see Fig. 5b) and the frequencies at which these peaks originates are known as plasma frequency. In these frequencies, $\varepsilon_1(\omega) = 0$ and $\frac{d\varepsilon_1(\omega)}{d\omega}$>0. At higher energy range, the amplitude of L(ω) gets larger as $\varepsilon_2(\omega)$gets smaller. After plasma frequency is attained, the compound tends towards transparency as$R(\omega) \rightarrow 0$. The highest peaks of reflectivity and loss function are positioned at 1.9184 eV, 2.7891 eV, 3.1157 eV and 21.5106 eV, 20.6126 eV, 21.40 eV respectively for Ti, Zr and Hf components of MCoSb. The static reflectivity $R(0)$and the static loss function $L(0)$are presented in Table 5. In the energy range between 0.0136 eV−1.7007 eV and between 23.088 eV−27.875 eV, L(ω) is very low indicating very less loss of electron energy due to scattering. R(ω) is also appreciably low indicating less reflection of the incident radiation in that energy range. Therefore, corresponding to $\varepsilon_2(\omega)$, $k(\omega)$, R(ω) and L(ω) results, we report that the HH compound MCoSb shows transparent properties in the energy range between 0.0136 eV−1.7007 eV and between 23.088 eV−27.875 eV.

In Fig. 6, the absorption and the conduction spectra of the compounds are shown. From the conduction spectra, we see that the threshold point occurs very close to 0 eV, indicating the narrow energy band gaps in the compounds. Therefore, the compounds are characterized as narrow band gap semiconductors which is evident from the band structure plots of the compounds reported earlier [11, 35, 36]. High peaks are observed both in the infrared as well as in the visible region of both the

Table 5. Calculated static dielectric constant $\varepsilon_1(0)$, optical band gap (ΔE_{OG}), static refractive index n(0), static reflectivity R(0) and static loss function L(0) for TiCoSb, ZrCoSb and HfCoSb.

Compound	$\varepsilon_1(0)$	ΔE_{OG}	*n(0)*	*R(0)*	*L(0)*
TiCoSb	21.505	0.775	4.64	0.416	0.000821
ZrCoSb	18.987	1.102	4.36	0.392	0.000809
HfCoSb	18.403	1.156	4.29	0.387	0.000796

https://doi.org/10.1016/j.heliyon.2019.e01155

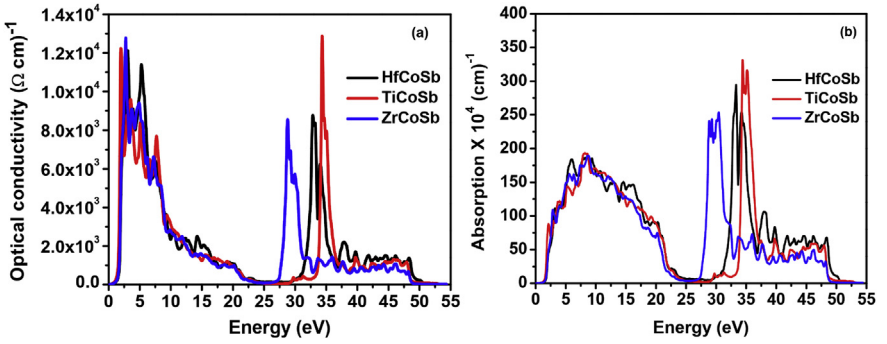

Fig. 6. (a) The conduction and (b) the absorption spectra of MCoSb.

conduction and absorption spectrum. Absorption spectra has peaks higher in the visible region and may be due to the transition between widely separated energy levels. In reference to the optical results obtained, it can be said that the compound ZrCoSb fails to show any type of optical behavior in the energy range 23−27 eV. The same holds for TiCoSb and HfCoSb, the energy range being much wider.

Unfortunately we could not compare our optical results due to lack of experimental as well as theoretical results. We have summarized our optical results in Table 5. HfCoSb results are in agreement with the optical results obtained by Coban et al [11].

4. Conclusion

We have presented the elastic and optical properties of half-Heusler MCoSb (M = Ti, Zr and Hf) using first principle methods. The Bulk modulus values calculated from ElaStic code are very close to the values calculated from Murnaghan's equation of state. The Debye's temperature are calculated within the DFT framework using the Lagrangian theory of elasticity as well as by using the quasiharmonic approximations. The values obtained from these two approaches are close to one another and also to the available experimental data. The optical band gaps calculated from the imaginary part of the dielectric function are found to be close to the energy band gap of the materials. This revels that the compounds acts as semiconductors to optical conduction as well as to electrical conduction. Further, the optical properties of the material varies according to the photon energies and can be beneficial to numerous applications like optoelectronic, thin film growth etc.

Declarations

Author contribution statement

Himanshu Joshi, Dibya P. Rai, Lalhriatpuia Hnamte, Amel Laref, R. K. Thapa: Conceived and designed the analysis; Analyzed and interpreted the data; Contributed analysis tools or data; Wrote the paper.

https://doi.org/10.1016/j.heliyon.2019.e01155

Funding statement

Himanshu Joshi and R. K. Thapa were supported by SERB Govt. of India (EMR/2015/001407). D. P. Rai was supported by DST New Delhi India & RFBR (DST/INT/RUS/RFBR/P-264). Amel Laref was supported by the Research Center of Female Scientific and Medical Colleges, Deanship of Scientifc Research, King Saud University.

Competing interest statement

The authors declare no conflict of interest.

Additional information

No additional information is available for this paper.

References

[1] T. Graf, C. Felser, S.S.P. Parkin, Simple rules for the understanding of Heusler compounds, Prog. Solid State Chem. 39 (2011) 1.

[2] I. Galanakis, P. Mavropoulos, P.H. Dederichs, Electronic structure and Slater−Pauling behaviour in half-metallic Heusler alloys calculated from first principles, J. Phys. D Appl. Phys. 39 (5) (2006) 765.

[3] P.J. Webster, K.R. Ziebeck, Alloys and Compounds of d-elements with Main Group Elements. Part 2, in: H.R.J. Wijn (Ed.), Landolt-Bornstein, New Series Group III, Vol. 32/c, Springer Berlin, 2001, pp. 64−414.

[4] F.G. Aliev, Gap at Fermi level in some new d- and f-electron intermetallic compounds, Physics B 171 (1991) 199−205.

[5] D.P. Rai, C. Sandeep, A. Shankar, M.P. Ghimire, R.K. Thapa, Electronic structure and magnetic properties of Co2yz(Y = Cr, Z = Al, Ga) type Heusler compounds: a first principle study, Int. J. Mod. Phys. B 26 (8) (2012) 1250071.

[6] H. Xiao, T. Hu, W. Liu, Y.L. Zhu, P.G. Li, G. Mu, J. Su, K. Li, Z.Q. Mao, Superconductivity in half-Heusler compound TbPdBi, Phys. Rev. B 97 (22) (2018) 224511.

[7] Fleur Legrain, Jesus Carrete, Ambroise van Roekeghem, Georg K.H. Madsen, Natalio Mingo, Materials screening for the discovery of new half Heuslers: machine learning versus ab initio methods, J. Phys. Chem. B 122 (2) (2018) 625−632.

https://doi.org/10.1016/j.heliyon.2019.e01155

[8] M. Born, Thermodynamics of crystals and melting, J. Chem. Phys. 7 (59) (1939) 591−603.

[9] Shu-Chun Wu, S. Shahab Naghavi, Gerhard H. Fecher, Claudia Felser, A critical study of the elastic properties and stability of Heusler compounds: phase change and tetragonal X_2YZ compounds, J. Mod. Phys. 09 (04) (2018) 83535.

[10] T. Sekimoto, K. Kurosaki, H. Muta, S. Yamanaka, Thermoelectric properties of (Ti,Zr,Hf)CoSb type half-Heusler compounds, Mater. Trans. 46 (7) (2005) 1481−1484.

[11] C. Coban, Y.O. Ciftci, K. Colakoglu, Structural, electronic, elastic, optical, and vibrational properties of HfXSb (X = Co, Rh, Ru) half-Heusler compounds: an ab initio study, Indian J. Phys. 90 (11) (2016) 1233−1241.

[12] R. Golesorkhtabar, P. Pavone, J. Spitaler, P. Puschnig, C. Draxl, ElaStic: a tool for calculating second-order elastic constants from first principles, Comput. Phys. Commun. 184 (2013) 1861−1873.

[13] P. Hohenberg, W. Kohn, Inhomogeneous electron gas, Phys. Rev. 136 (1964) B864.

[14] W. Kohn, L.J. Sham, Self-consistent equations including exchange and correlation effects, Phys. Rev. 140 (1965) A1133.

[15] M.A. Blanco, E. Francisco, V. Luana, GIBBS: isothermal-isobaric thermodynamics of solids from energy curves using a quasi-harmonic Debye model, Comput. Phys. Commun. 158 (2004) 57−72.

[16] A. Otero-de-la-Roza, D. Abbasi-Pérez, V. Luana, Gibbs2: a new version of the quasiharmonic model code. II. Models for solid-state thermodynamics, features and implementation, Comput. Phys. Commun. 182 (2011) 2232−2248.

[17] M. Born, K. Huang, Dynamics Theory of Crystal Lattices, Oxford University Press, 1954.

[18] J. Perdew, K.P. Burke, M. Ernzerhoff, Generalized gradient approximation made simple, Phys. Rev. Lett. 77 (1996) 3865.

[19] P. Blaha, G.K.H. Madsen, D. Kvasnicka, J. Luitz, WIEN2K, an Augmented Plane Wave Plus Local Orbitals Program for Calculating crystal Properties (Vienna, Austria), 2008.

[20] F.D. Murnaghan, The compressibility of media under extreme pressures, Proc. Natl. Acad. Sci. U.S.A. 30 (1994) 5390.

 https://doi.org/10.1016/j.heliyon.2019.e01155

[21] Yu. Stadnyk, Yu. Gorelenko, A. Tkachuk, A. Goryn, V. Davydov, O. Bodak, Electric transport and magnetic properties of $TiCo_{1-x}Ni_xSb$ solid solution, J. Alloy. Comp. 329 (2001) 37−41.

[22] T. Sekimoto, K. Kurosaki, H. Muta, S. Yamanaka, IEEE- 24th International Conference on Thermoelectrics, 2005.

[23] Takeyuki Sekimoto, Ken Kurosaki, Hiroaki Muta, Shinsuke Yamanak, Thermoelectric and thermophysical properties of TiCoSb, ZrCoSb, HfCoSb prepared by SPS, Mater. Trans. 46 (2006) 7.

[24] G. Melnyk, E. Bauer, P. Rogl, R. Skolozdra, E. Seidl, Thermoelectric properties of ternary transition metal antimonides, J. Alloy. Comp. 296 (2000) 235−242.

[25] D.T. Morelli, G.A. Slack, High Lattice Thermal Conductivity of Solids, Springer, New York, USA, 2006.

[26] W. Voigt, Lehrbuch der kristallphysik (mit ausschluss der kristalloptik), B.G. Teubner, Leipzig, Berlin, 1910.

[27] A. Reuss, Berechnung der Fließgrenze von Mischkristallen auf Grund der Plastizitätsbedingung für Einkristalle, ZAMM-J. Appl. Math. Mech 9 (1929).

[28] R. Hill, The elastic behavior of a crystalline aggregate, Proc. Phys. Soc. 65 (1952) 349−354.

[29] U.F. Ozyar, E. Deligoz, K. Colakoglu, Systematic study on the anisotropic elastic properties of tetragonal XYSb (X = Ti, Zr, Hf; Y = Si, Ge) compounds, Solid State Sci. 40 (2015) 92−100.

[30] O.L. Anderson, A simplified method for calculating the Debye temperature from elastic constants, J. Phys. Chem. Solid. 24 (1963) 909−917.

[31] H.A. Kramers, La diffusion de la lumiere par les atomes, Atti Cong. Intern. Fisica, (Transactoions of Volta Centenary Congress) Como 2 (1927) 545−557.

[32] P. Ravindran, A. Delin, B. Johansson, O. Eriksson, Electronic structure, chemical bonding, and optical properties of ferroelectric and antiferroelectric $NaNO_2$, Phys. Rev. B 59 (1999) 591776.

[33] Shanming Li, Huaizhou Zhao, Dandan Li, Shifeng Jin, Lin Gu, Synthesis and thermoelectric properties of half-Heusler alloy YNiBi, J. Appl. Phys. 117 (2015) 205101.

https://doi.org/10.1016/j.heliyon.2019.e01155

[34] G.K.H. Madsen, P. Blaha, K. Schwarz, E. Sjöstedt, L. Nordstrom, Efficient linearization of the augmented plane-wave method, Phys. Rev. B 64 (2001) 195134.

[35] Gaili Sun, Yuanyuan Li, Xinxin Zhao, Yiming Mi, Lili Wang, First-Principles investigation of the effect of M-doped (M = Zr, Hf) TiCoSb half-Heusler thermoelectric material, J. Mater. Sci. Chem. Eng. 3 (2015) 78−86.

[36] Jiong Yang, Huanming Li, Ting Wu, Wenqing Zhang, Lidong Chen, Jihui Yang, Evaluation of half-Heusler compounds as thermoelectric materials based on the calculated electrical transport properties, Adv. Funct. Mater. 18 (2008) 2880−2888.

https://doi.org/10.1016/j.heliyon.2019.e01155